Cover Picture: Mechanistic Origin of the Vibrational Coherence Accompanying the Photoreaction of Biomimetic Molecular Switches (Chem. Eur. J. 48/2012)

ARTICLE *in* CHEMISTRY - A EUROPEAN JOURNAL · NOVEMBER 2012

Impact Factor: 5.73 · DOI: 10.1002/chem.201201430 · Source: PubMed

DOI: 10.1002/chem.200((will be filled in by the editorial staff))

Mechanistic Origin of the Vibrational Coherence Accompanying the Photoreaction of Biomimetic Molecular Switches

Jérémie Léonard[a], Igor Schapiro[b], Julien Briand[a], Stefania Fusi[b], Riccardo Rossi Paccani[c], Massimo Olivucci[b],[c], Stefan Haacke*[a]

Abstract: The coherent photo-isomerization of a chromophore in condensed phase is a rare process where light energy is funneled into specific molecular vibrations during electronic relaxation from the excited to the ground state. In this work we employ ultrafast spectroscopy and computational methods to investigate the molecular origin of the coherent motion accompanying the photo-isomerization of indanylidene-pyrroline (IP) molecular switches. UV-Vis femtosecond transient absorption gives evidence for an excited and ground state vibrational wavepacket which appears as a general feature of the IP compounds investigated. In close resemblance to the coherent photo-isomerization of rhodopsin, the wavepacket depopulates the excited state impulsively, and is remarkably preserved in form of damped, low-frequency oscillations in the ground state. Semi-classical trajectories are employed to investigate the reaction mechanism in the excited state and after decay at the conical intersection. Their analysis shows that coupled double-bond twisting and ring-inversions already populated during the excited state relaxation induce periodic changes in π-conjugation that are responsible for the observed ground state oscillations in the absorption band. The IP compounds appear as photomechanical transducers converting a significant amount of the photon energy into kinetic energy delivered in a few specific reactive modes. The presented mechanism opens new perspectives for energy transduction at the molecular level with applications to the design of efficient molecular devices.

Keywords: keyword 1 • keyword 2 • keyword 3 • keyword 4 • keyword 5

Introduction

Light-driven molecular switches (photoswitches) produce mechanical work at the molecular scale in response to an optical excitation and can be used as building blocks for man-tailored nanoscale molecular devices [1]. Photoswitches are found in nature where their function is to modulate the biological activity of various photosensitive proteins. This is the case in bovine Rhodopsin (Rh), the dim-light visual pigment of superior animals, with the protonated Schiff base of 11-*cis*-retinal (PSBR) as a "natural" photoswitch. PSBR triggers the visual cycle by undergoing one of the fastest (200 fs [2]) and most efficient (quantum yield of 67% [3]) double bond photoisomerization ever observed. Unraveling the mechanistic details governing such an event [4] would allow the design and preparation of artificial photoswitches with targeted properties.

Following a so-called biomimetic approach, a new family of molecular switches based on the indanylidene-pyrroline (IP) framework has been designed and synthesized to mimic the photoisomerization of PSBR in Rh [5]. The theoretical and experimental investigation of one of these switches, the *p*-methoxy N-alkylated IP cation (MeO-NAIP) [6] of Figure 1, revealed an S_1 energy landscape and an isomerization speed similar to the ones observed in Rh. Indeed, the non-radiative decay from the first excited state (S_1) to the ground state (S_0) is mediated by a conical intersection (CI), which is a real crossing between the S_1 and S_0 potential energy surfaces [7]. Simulations suggest that the speed and quantum yield of this process is governed by the shape of the potential energy surfaces and by the topology of the CI [8], influenced by the environment [9].

In the context of designing artificial photoswitches with *directed* photo-energy conversion the occurrence of vibrational coherences is of high relevance since they indicate that the molecular kinetic energy is located in a small set of specific vibrational modes, possibly driving the reaction. The process manifests itself in terms of non-exponential reaction kinetics, in particular a modulated absorption signal displaying a damped oscillatory behavior. Rh provides the only known example of such coherent photoisomerization occurring in Nature [10], but given the complexity of Rh the mechanistic details are only partly understood A zwitterionic MeO-NAIP derivative (R'=COO(-) in Figure 1) labeled ZW-NAIP was found to display a temporally oscillating signal similar to Rh [11] and, to the best of our knowledge, it is the only synthetic system presently reported to do so. Thus, IP photoswitches appear to be model systems useful for both the experimental and theoretical investigation of the mechanism of biological photoisomerization since it is possible to avoid the costly sample preparation and difficult modeling of visual pigments.

In this work we use complementary experimental and computational methods to investigate the mechanism responsible for the appearance of vibrational coherence upon irradiation of two cationic (R'=H) IP switches. Accordingly, we perform transient absorption measurements on a methylated (MeO-NAIP with R=Me) and a protonated (MeO-NHIP with R=H) IP (see Figure 1). We show that the coherent dynamics observed in ZW-NAIP [11-12] is conserved in MeO-NAIP and MeO-NHIP demonstrating, most

[a] Dr J. Léonard, Dr. J. Briand, Prof. S. Haacke
Institut de Physique et Chimie des Matériaux de Strasbourg, IPCMS-DON
CNRS – Université de Strasbourg
23 rue du Loess, 67034 Strasbourg, France
Fax: (+33) 3 88 10 7245
E-mail: haacke@unistra.fr

[b] Dr I. Schapiro, Prof. M. Olivucci,
Chemistry Department, Bowling Green State University
Bowling Green, OH 43403, USA

[c] Dr S. Fusi, Dr R. R. Paccani, Prof. M. Olivucci,
Dipartimento di Chimica, Università degli Studi di Siena
via Aldo Moro 2, I-53100 Siena, Italy

Supporting information for this article is available on the WWW under http://www.chemeurj.org/ or from the author.

importantly, that the mechanism driving the coherent energy conversion is a general feature of the IP family. We also investigate the mechanism of the MeO-NHIP photoreaction by computing 2 ps quantum-mechanics/molecular-mechanics (QM/MM) scaled-CASSCF/Amber semi-classical trajectories which significantly expand the sub-ps studies reported before [4c, 13]. The S_0 relaxation simulated over ca. 1.5 ps after the CI shows pronounced oscillations of the S_0-S_1 energy gap which qualitatively replicates the observed oscillation in excitation energies. These oscillations are shown to be due to coupled double-bond twisting and ring deformations affecting the overlap between two distinct π-systems of the switch framework.

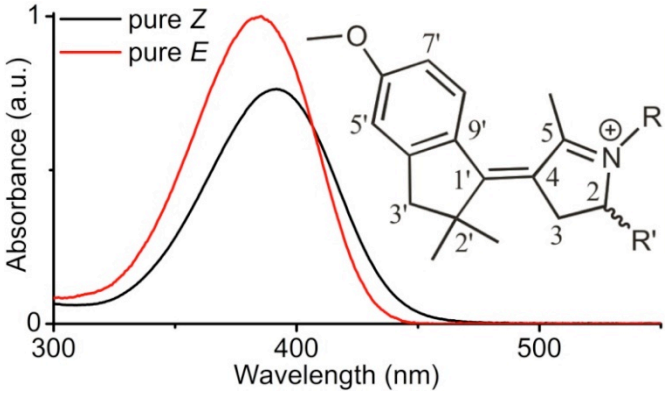

Figure 1: Absorption spectra of the pure *E* and *Z* solutions of MeO-NAIP (R=Me and R'=H, Cl^- as counterion) in methanol and chemical structure of the cationic *Z*-MeO-NAIP, *Z*-MeO-NHIP (R=H, R'=H) and *Z*-ZW-NAIP (R=Me, R'=COO^-).

Experimental Results

Figure 2 displays an overview of the transient absorption data recorded over the first 1.5 ps for the methylated *Z*-MeO-NAIP in methanol. At short time delays (≤ 250 fs), we observe the spectroscopic signature of the S_1 state. It is essentially composed of stimulated emission (SE) producing a negative contribution (ΔA <0, in blue) from 450 nm to above 700 nm, and of excited state absorption (ESA) producing a positive contribution (ΔA > 0, in red) from 440 nm down to 300 nm. The latter signal happens to overlap with the ground state bleach (GSB, ΔA <0 between 350 and 420 nm) such that around 370 nm the GSB signal overcomes the ESA signal, resulting in an overall negative ΔA at early times. The spectroscopic signatures of the S_1 state are very short-lived (<0.3 ps) [6]. Like in the case of ZW-NAIP [11-12], they are followed by a very broad photoproduct absorption band (PA, ΔA >0) which emerges impulsively around 0.3 ps from 420 nm to 700 nm, and rapidly narrows and blue-shifts into the 430-nm band seen to last from ~ 0.3 ps to 1.5 ps and beyond.

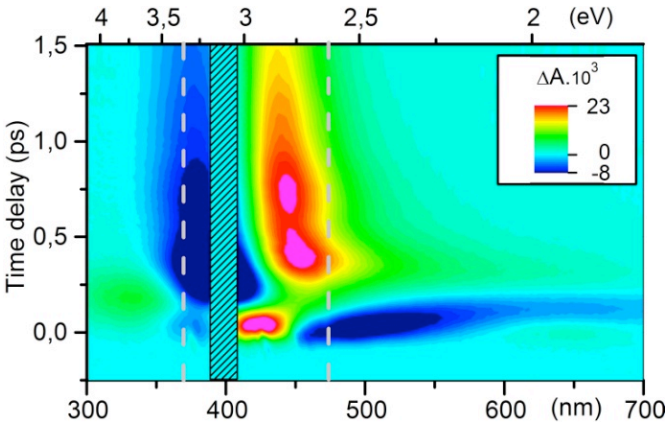

Figure 2: Transient absorption changes (in false color scale) of the methylated *Z*-MeO-NAIP in methanol after excitation at 400 nm, as a function of wavelength (in nm and eV) and time delay between excitation and probe pulses (in ps). The crossed-out region is disregarded due to enhanced noise caused by the excitation beam scattering. Two vertical dashed lines indicate the wavelengths (370 nm and 475 nm) at which oscillatory features are most pronounced (see Figure 3B).

Figure 3 displays kinetic traces extracted at several wavelengths from the data displayed in Figure 2. Figure 3A illustrates the dynamic spectral shift observed in the ESA signal, which appears instantaneously around 420 nm, but with a delayed onset in the UV-most part of the observation window (320 nm). Similarly, at times ≥ 0.25 ps, the PA band impulsively appears with a delayed onset in the red most part of the data (positive signal at ~0.3 ps in the 650-nm trace) and rapidly blue-shifts, causing the first maximum in the 475-nm trace around 0.35 ps, and a local maximum in the 370-nm trace around 0.5 ps, as shown in Figure 3B (labels 1 and 2). An oscillatory behavior is observed in the red (475 nm) and in the blue (370 nm) of the photoproduct absorption band, with opposite phases (Figure 3B, inset).

The entire transient absorption signature of *Z*-MeO-NAIP is very close to that reported for *Z*-ZW-NAIP [11-12]. Hence the same interpretation holds: a vibrational wave packet is created in the excited state, highlighted by the ESA spectral shift. In the blue-most part of the observation window, the delayed ESA reaches its maximum at a pump-probe delay of 190 ± 10 fs. This is the latest spectroscopic signature of the molecules in the excited state, before crossing the CI. Note that the UV part of the ESA lives longer than the fluorescence emission which was reported to exhibit a biphasic decay with a dominant component faster than 40 fs [6]. Then, the spectroscopic signature of the wave packet is temporarily lost while it evolves in the vicinity and through the CI. Like in ZW-NAIP or in Rh [4b, 14], the earliest signature of the wavepacket after crossing the CI is observed in the red to infrared region (up to λ>700 nm). Here, the PA band impulsively appears and reaches its maximum after 330 ± 15 fs in the 650 nm trace (Figure 3A). The

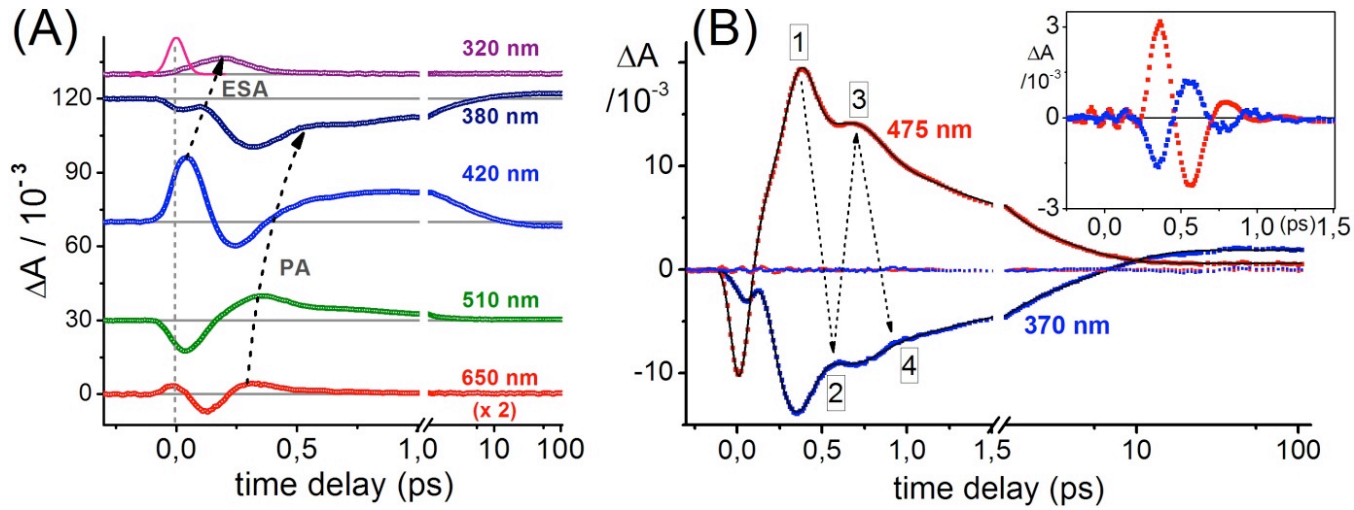

Figure 3: Coherent dynamics of *Z*-MeO-NAIP. (A) Selection of kinetic traces extracted from the data displayed in Figure 2. At early times the ESA signature overlaps with the GSB signal (traces at 420 and 380 nm). The Gaussian curve overlapped with the 320-nm trace has a FWHM of 80 fs, representative of the instrument response function (IRF). The curved, dashed arrows illustrate the dynamic spectral shifts of the ESA and PA bands. (B) The 370-nm (blue) and 475-nm (red) traces show the most pronounced oscillatory behavior. The labels 1 to 4 and dashed arrows highlight the positive absorption feature observed alternatively in the red and blue sides of the photoproduct absorption band. The global fitting of both traces (black lines, see the Supporting Information) allows us to extract the anti-phased, oscillatory components displayed in the inset.

vibrational wavepacket further evolves and oscillates around the equilibrium position in the ground state thus producing the oscillations observed in the 475 and 370 nm traces (Fig 3B). An appropriate fitting procedure allows us to extract the oscillatory component of the two traces and to measure their period and damping time (see the Supporting Information). In the case of *Z*-MeO-NAIP in methanol, they are 490 fs (corresponding to a 70 cm^{-1} frequency) and 180 fs, respectively. Beyond 1.5 ps, further evolution is dominated by incoherent vibrational relaxation as already reported [6]. Note that, as shown in detail elsewhere[11-12], the wavepacket observed in S_0 originates from a vibrational coherence created in S_1 and preserved through the CI. However, since both isomers have similar absorption spectra, it is not possible to determine whether the wave packet is observed along the reactive (*E*) or non-reactive (*Z*) pathway. On the other hand, the fact that *Z* to *E* isomerization yield is not more than ~21% for MeO-NAIP [5a, 6]. points to a signal coming from the reactant (*Z*) reconstitution.

The above experimental investigation is completed by two identical experiments carried out on the *E* form of the same molecule and on the *Z* form of the protonated MeO-NHIP, in the same solvent. In the first case, we investigate the dynamics of the reverse process, and in the second case, the influence of the nature of the N-substituent. Figure 4 and Table 1 summarize the three experiments. In all cases, the ESA signal shows a delayed rise in the UV and reaches its maximum at 200 fs (320-nm traces). This indicates a very similar excited state dynamics. At 550 nm, the maximum photoproduct absorption signal is observed at ~300 fs for MeO-NHIP, and at ~330 fs for both *Z*- and *E*-MeO-NAIP, indicating a slightly faster decay for the N-protonated molecule. Finally, in the three experiments, similar S_0 oscillations are observed at 460 nm. However, we note that i) the oscillation period is shorter (330 fs) in the case of MeO-NHIP (see Table 1) and ii) although less pronounced in the case of the *E*-MeO-NAIP, an oscillatory behavior is still present with similar frequency as in the forward direction (see the Supporting Information).

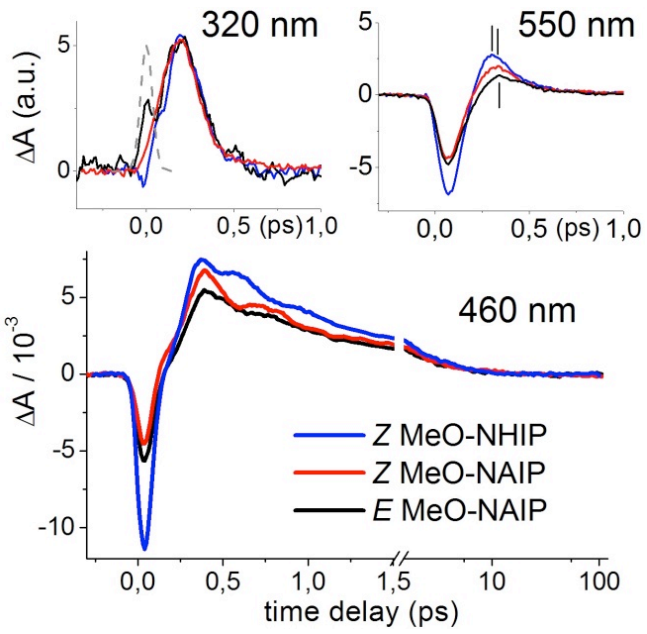

Figure 4: Comparison between the transient absorption kinetics of *Z*-MeO-NAIP (red), *E*-MeO-NAIP (black) and *Z*-MeO-NHIP (blue) at three selected wavelengths. At 320 nm: delayed ESA with a maximum at 200 fs. The dashed grey Gaussian curve represents the IRF. The differences in the ±100-fs window around time zero are due to a spurious solvent contribution. At 550 nm: short-lived SE followed by the impulsive rise of the S_0 wavepacket signature. Three vertical cursors pinpoint slight differences in the arrival time (~300 fs for MeO-NHIP and ~330fs for *Z*- and *E*-MeO-NAIP). At 460 nm: SE followed by S_0 oscillations with sample-dependent frequencies and damping.

Table 1: Observation times in fs of (a) the maximum of the ESA signature at 320 nm and (b) the maximum of the PA signature at 550 nm. Oscillation period (c) in fs and in brackets in cm^{-1} and damping (d) in fs, obtained by fitting the photoproduct signal at 460 nm (see the Supporting Information).

	(a)*	(b)*	(c)**	(d)**
Z-MeO-NAIP	200	330	490 (70)	180
E-MeO-NAIP	200	330	570 (60)	220
Z-MeO-NHIP	200	300	330 (100)	260
Z-ZW-NAIP [12]	200	395	650 (50)	330

* accuracy on experimental time delays is estimated to be ± 20 fs, limited by our ability to correct for the white light group velocity dispersion [11].

** accuracy on the time constants extracted from the fitting procedure is estimated to be ~10 to 15 %.

Computational Results

We compute (see Computational Methods) two QM/MM semi-classical trajectories starting from the Franck-Condon (FC) structures of the computationally more tractable MeO-NHIP system in methanol. Trajectory I describes the *Z* to *Z* internal conversion mediated by the CI (an aborted *Z* to *E* isomerization) whereas trajectory II describes a successful *E* to *Z* isomerization (cf. Scheme 1). The excited state branches ($I_{Z\rightarrow CI}$ and $II_{E\rightarrow CI}$) of I and II lead to two different CIs, $CI_{Z\rightarrow Z}$ and $CI_{E\rightarrow Z}$ which belong to the same intersection space. After the CIs, the trajectories evolve along the same S_0 *Z*-MeO-NHIP potential energy valley from opposite directions.

Due to the low quantum yield of the *Z* to *E* photoisomerization, *Z* to *Z* internal conversion also prevails experimentally. Therefore the analysis of the two trajectories, that are assumed to represent the average motion of reacting populations, is expected to provide an atomic-level understanding of the observed oscillatory features. We will see that the character of the structural relaxation is very similar along both trajectories, and does not depend critically on the corresponding initial conditions.

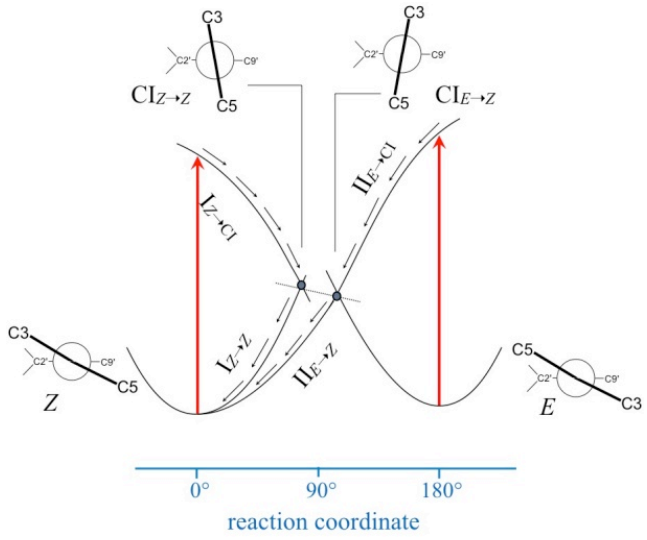

Scheme 1

From the FC point to the CIs, both trajectories show a steep decrease of the S_1 potential energy and similar geometrical evolutions (see Figure 5A and the movies in the Supporting Information). The C4=C1' exocyclic double bond undergoes an immediate elongation of ca. 0.2 Å, and essentially becomes a single bond. Subsequently the rotation around the same bond begins as shown by the C5–C4=C1'–C9' dihedral angle. This rotation constitutes a dominant contribution to the relaxation coordinate. It is coupled with the concerted inversions of the indanylidene (left) and pyrrolinium (right) rings illustrated in Figure 5B, as evidenced by the changes of the C3'-C2'-C1'-C9' and the C5-C4-C3-C2 dihedral angles. The ring inversions contribute to the torsion around C4=C1' while minimizing the required space and conserving the position of the center of mass of both rings, during the early stage of the isomerization dynamics. In the case of ZW-NAIP, we showed [5b] that they take place in both the excited-state trajectory and the minimum energy path, indicating that they are driven by the S_1 force field and therefore are part of the reaction coordinate.

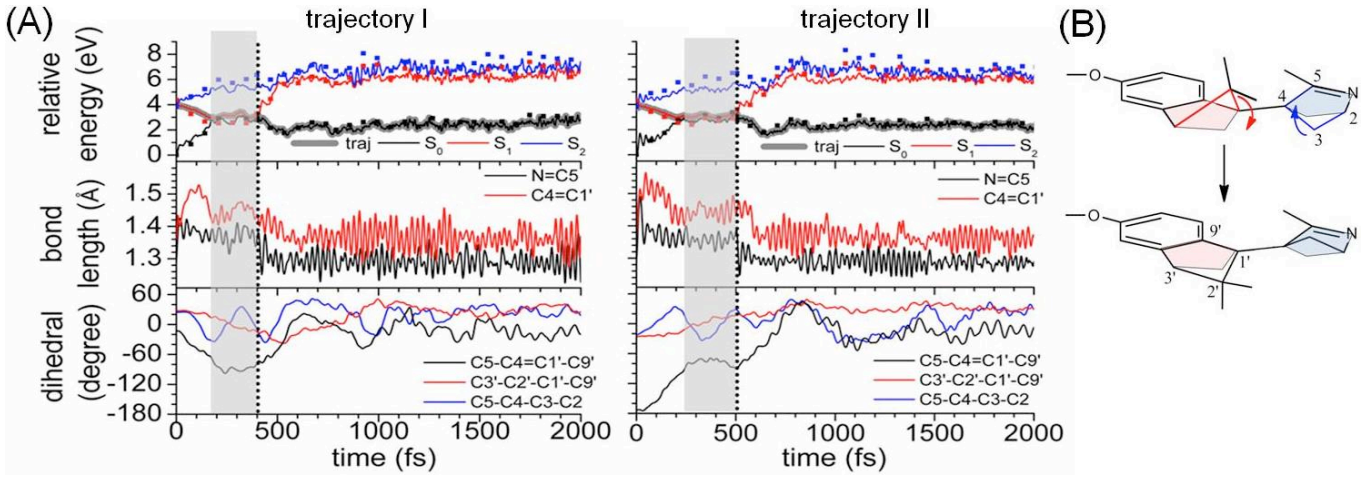

Figure 5: (A) Scaled-CASSCF trajectories I and II. The shaded areas indicate the regions where the S_0-S_1 energy gap remains below 0.3 eV before the computed hop (dashed vertical lines) at 400 fs for trajectory I, and 500 fs for trajectory II. Top: CASSCF energies (solid lines) and CASPT2 values (dots) of the three lowest states. The grey thick lines represent the reacting electronic state of the molecule. Middle: Selected bond lengths. Bottom: Selected dihedral angles showing the twisting around the exocyclic double bond (black), the indanylidene ring inversion at C2' (red), and the pyrrolinium ring inversion at C3 (blue). (B) Illustration of the contribution of the concerted ring inversions at C2' and C3 to the C1'=C4 twisting, along the excited state trajectory of *Z*-MeO-NHIP. Similar observations are made along trajectory II (see Movies in the Supporting Information)

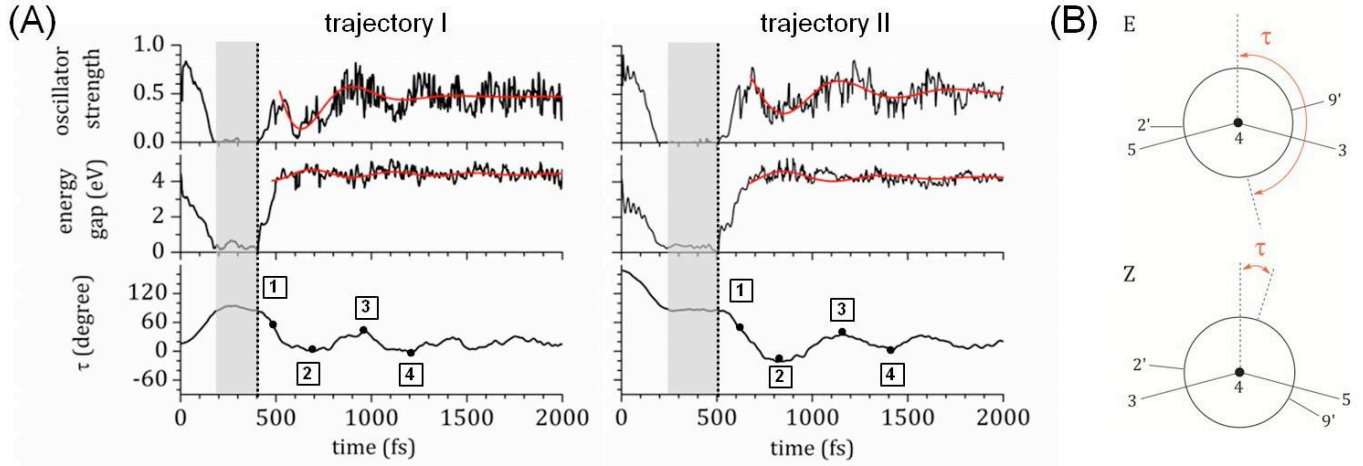

Figure 6: (A) Analysis of the oscillations in trajectories I (left) and II (right). Top: S_1-S_0 oscillator strength. Middle: energy gap. Bottom: geometrical τ parameter. . After the hop, the labels 1 to 4 defined in Figure 3B are associated to the local extrema of τ and of the S_1-S_0 energy gap along the trajectories. (B) Definition of the τ parameter describing the conjugation of the π-system.

In ~ 200 fs the S_1-S_0 energy gap has dropped to almost zero and the C5–C4=C1'–C9' dihedral angle has changed by ~90° in both trajectories. However, in this region of strong coupling, the surface hopping algorithm used in our modeling does not produce a hop until 400 fs (trajectory I) or 500 fs (trajectory II). Although it has been validated by previous QM and QM/MM calculations (see the Supporting Information) this algorithm may overestimate the excited state lifetimes. Here we assume that the actual hop occurs between the first S_0-S_1 touching and the computed hop (190-400 fs and 210-500 fs for trajectory I and II, respectively). We will see that the main features of the S_0 relaxation are essentially the same in both trajectories (see below), meaning that they do not critically depend on initial conditions. For this reason, we also assume that the computed trajectories provide a relevant mechanistic description after the hop.

In less than 100 fs after the hop, the C4=C1' bond shortens and recovers its double bond character in both trajectories. However, while in the first case, the C5-C4=C1'-C9' dihedral twists back towards the original *Z* conformation in ~150 fs, in the second case it twists further, completing the isomerization. Both trajectories have been pursued until 2 ps and clearly display equilibration of the C5-C4=C1'-C9' dihedral around the *Z* equilibrium angle (-12°) together with dissipation of vibrational energy to the surrounding solvent molecules (see movies in the Supporting Information).

In Figure 6 A, we plot the S_1-S_0 energy gap and oscillator strength computed along the trajectories. The small 3-21G basis set used here (see Methods and Supporting Information), only allows for a qualitative comparison of the computed energy gap with the observed absorption maxima. In the first 100 fs after vertical excitation the S_1-S_0 energy gap drops by a factor of ~2, while the oscillator strength still has significant magnitude (>0.5). This is in line with the observed stimulated emission extending very far towards the infrared (λ>700 nm, see Figure 2). In the next ~50 fs, the oscillator strength drops to zero, reproducing the very rapid vanishing of the SE. After the hop, the oscillator strength suddenly recovers and the energy gap rises again. This reproduces the earliest, far red-detuned, rapidly blue shifting photoproduct absorption observed after ~300 fs at λ>550nm. The simulations thus capture, in essence, important experimental features of the molecular wavepacket, as it leaves the FC region and passes through the CI.

Further S_0 evolution is characterized by the π-phase-shifted oscillations of the oscillator strength and of the S_1-S_0 energy gap (see Figure 6 and discussion below). This computed behavior is in line with the positive absorption feature observed in S_0 absorption band (see Figure 3B, labels 1 to 4). It qualitatively reproduces the relative amplitudes of the observed oscillations, which are larger in the low-energy side (475 nm) than in the high-energy side (370 nm) of the PA band (Figure 3B inset). The fitting of an exponentially damped sine function to the energy gap oscillation reveals an oscillation period of 420 fs and 520 fs for trajectory I and II respectively. Its order of magnitude is therefore in agreement with the 330 fs observed for *Z*-MeO-NHIP (490 to 570 fs for MeO-NAIP, see Table 1), given i) the experimental uncertainty and ii) the constraints imposed on the model due to computational costs. For instance, the 3-21G basis set imposes a longer and weaker double bond with respect to better but more expensive basis 6-31G* (See discussion in Supporting Information). This could be at the origin of the overestimated oscillation period.

Discussion

We now use the outcome of the modeling to provide a mechanistic explanation for the origin of the observed coherent motion. In order to draw a connection between the geometrical deformations and the S_1-S_0 excitation energy we need to understand their influence on the electronic structure and in particular on the π-conjugation. We derive a geometrical parameter τ which is the angle between the two C4 and C1' p-orbital vectors [15] (see Figure 6B and definition in the Supporting Information). It relates to the overlap of the p-orbital lobes across the C4=C1' isomerizing double bond, therefore to the strength of the π-bonding. A small overlap (τ approaching 90°) corresponds to a weak bonding and a smaller S_1-S_0 energy gap, whereas a large overlap (τ approaching 0° or 180°) corresponds to a strong bonding and a larger energy gap. All geometrical deformations affecting τ will affect the π-conjugation. These include not only the twisting about the reactive double bond but also, for instance, the ring inversions at C2' and C3. Notice that in addition, the C4 and C1' pyramidalizations (which are dynamically coupled to the ring inversions at C2' and C3) affect the π-conjugation but, in principle, do not change the τ angle. Importantly, Figure 6 shows that after the hop, the time evolution of τ correlates with that of the energy gap.

Based on the consistency between the computed and observed oscillatory behavior in the energy gap, we assign the local extrema of τ and of the energy gap (Figure 6), to the points labeled 1 to 4 in the transient absorption data (Figure 3). The corresponding

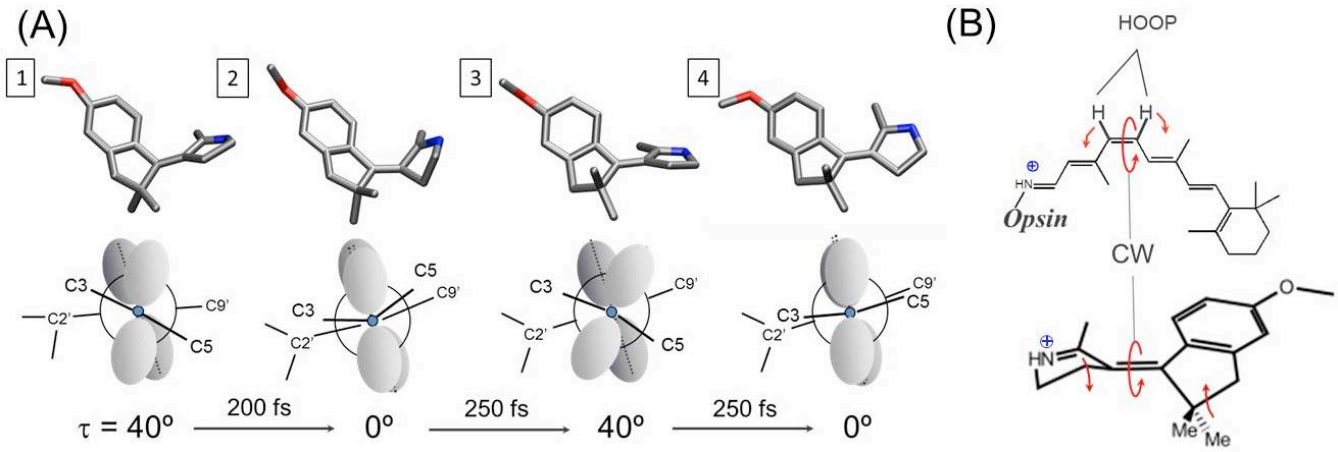

Figure 7**:** (A) Trajectory I geometries corresponding to the local extrema 1 to 4 (Figure 6 A) of the τ angle along the ground state relaxation. (See the corresponding figure for trajectory II in the Supporting Information). Top: While the indanylidene ring undergoes one inversion at C2' from structure 1 to 4, the pyrrolinium ring periodically moves out-of-plane while deforming. Bottom: corresponding Newman projections along the C4-C1' axis and τ angle values. (B) Schematic representation of the HOOP motion and ring-inversion accompanying the clockwise (CW) isomerization in Rh and IPs, respectively.

molecular structures are extracted from the model and displayed in Figure 7 for trajectory I (for trajectory II see Figure S8). Among many structural deformations, a global, damped, periodic out-of-plane motion of the pyrrolinium ring is seen (structure 1 is similar to 3 and structure 2 to 4, see also movies in the Supporting Information). The periodic change involves double bond twisting and ring inversions that in turn induce the modulation of τ. About 100 fs after the hop (label 1), the value of τ indicates a strong alteration of the π-conjugation which is still mainly due to the significant twisting around C4=C1' as shown in Figure 5 A. After another 200 fs (label 2) and further, close inspection of the geometrical changes along the computed trajectories shows that the modulation in τ is mainly caused by the deformations of both rings. In particular, the inversion motion of the pyrrolinium ring is predominantly involved as is best illustrated by the C5-C4-C3-C2 dihedral angle (see Figure 5). Instead the pyramidalization of C4 and C1' remains limited, explaining why the τ angle alone is relevant to quantify the strength of the π-bonding.

Conclusion

The results above show that the IP switches reproduce different spectro-temporal features of the rhodopsin's ultrafast photo-reaction [2, 4b]. In particular, the *Z*-MeO-NAIP, *E*-MeO-NAIP and *Z*-MeO-NHIP photoswitches display important coherent vibrational dynamics. Together with results on a third compound, the zwitterionic ZW-NAIP [11-12], the present work establishes that in IP switches a part of the photon energy is effectively funneled into specific low-frequency S_0 modes. This effect is apparently not sensitive to (i) the state of the counterion (in solution or intramolecular), (ii) the nature of the N substituent (Me vs. H), (iii) the substitution in position 2 (-COO(-) vs. H), (iv) the increase in steric hindrance and hydrogen bonding capability and (v) the nature (viscosity) of the solvent (MeOH vs. decanol, [12]). Therefore the observed vibrational coherence seems to be a rather general manifestation of the geometrical and electronic structure of the IP chromophore framework. To the best of our knowledge, this is a unique finding for any class of molecules, mimicking the hitherto unparalleled coherent photo-isomerization observed in Rh.

The computational investigations of the MeO-NHIP photoreactions via QM/MM semi-classical trajectories produce low-frequency oscillations in the S_1-S_0 energy gap that provides a basis for the mechanistic interpretation of the observed absorption features. The simulation, which does not appear sensitive to qualitative changes in the initial conditions (i.e. when starting from the *E* or *Z* isomer), indicates that coupled double bond torsion and ring inversions modulate the conjugation between two π-subsystems interacting across the isomerizing bond. We assign the observed vibrational coherences to these modes that, according to our trajectories, are promptly populated after leaving the Franck-Condon region and during the S_1 relaxation. Remarkably, these ring inversions appear to be a lower frequency analogue of the hydrogen-out-of-plane (HOOP) modes in Rh (cf. fig. 7B), which were also shown to contribute to the reaction coordinate and to be activated immediately after light absorption [4c, 16].

Our combined computational and spectroscopic study provides unprecedented mechanistic details in the description of the photoisomerization of sizable organic chromophores in the condensed phase. We believe that further research efforts focusing on the IP model systems may deliver fundamental insights on the relationship between photoreaction speed, vibrational coherence, and photoreaction yield opening new perspectives for the design of systems capable of funneling the photon energy into specific modes.

Experimental Section

In the dark at room temperature, in methanol with a chloride counterion, MeO-NAIP is in the *Z* isomer form at >95%. Upon illumination at 455 nm, it is possible to accumulate the *E* isomer up to nearly 90% (see the Supporting Information). The *E* isomer is then stable over hours, before thermal relaxation back to the *Z* form. The protonated MeO-NHIP is also in almost pure *Z* form under the same conditions and displays the same absorption spectrum as *Z*-MeO-NAIP (not shown). The set-up for transient absorption spectroscopy as well as data processing and analysis techniques were described previously in detail [6, 11]. In short, the pump beam is at 400 nm, obtained by second harmonic generation from the 800-nm, 40-fs fundamental beam of an amplified, 5-kHz, laser system. A white light continuum is generated by focusing 2 μJ of the 800 nm beam in a vertically oscillating, 1-mm thick CaF_2 plate. It is used as a broadband probe pulse (300-1100 nm). The pump pulse power density is set to ~0.5 mJ/cm^2, within the linear regime of excitation. Transient absorption data of the pure solvent is systematically recorded and subtracted from the raw data [11] obtained for the switches in solution. Further data processing is made to correct the effects of group velocity dispersion (chirp) in the white light continuum [11] such that the zero time delay is defined within ±20 fs over the entire detection spectral window. The time resolution is ~80-fs.

Computational Methods

QM/MM semi-classical trajectories were computed using the Molcas [17] 7.5 developer version and Tinker [18] 4.2 programs. Each photoswitch is placed in a solvent box with methanol molecules and one chloride counterion, described by the Amber [19] force field. The dimension of the box was chosen such that each atom of the switch is at least 10 Å away from the boundary. The three-root state-average CASSCF(10,10)/3-21G level of theory is employed to describe the switch quantum mechanically. All conjugated π-type orbitals are included within the active space of 10 electrons in 10 orbitals except for the lone pair on the hydroxyl-oxygen (See Figure S4). For the IP switches, it is impossible to compute the trajectories at the MS-CASPT2 level due to the high computational cost and to the lack of efficient analytical gradients. However, the CASSCF energy profile can be scaled by a calibrated factor to approximate the corresponding CASPT2 S_1 profile [13]. The resulting scaled-CASSCF potential provides a MS-CASPT2-like excited-state force field and therefore time scales. In this work we use the scaling factor α=0.535 employed by Melloni et al. [5b] for ZW-NAIP. The use of the 3-21G basis set is imposed by the computational demand of the 2-ps trajectory calculations. The description provided by this relatively small basis set has been shown to be adequate for mechanistic investigations (see the Supporting Information) although it impairs the quantitative comparison of excitation energies and reaction time scale. The FC geometries for trajectory computations are obtained from QM/MM energy-minimization on the ground state. The methanol molecules of the first solvation shell only (e.g. with at least one atom within 4 Å distance to the switch) are relaxed using the microiteration method [20]. The same active space and basis set, as for the geometry optimization, are used. The velocity Verlet algorithm [21] and the forces obtained from the QM/MM setup are used to propagate the Newton's equations of motion over successive time steps of 1 fs. Along the trajectories, non-adiabatic transitions between the different states are detected by a surface hopping algorithm.[22] Finally, the comparison with the observed time evolution of the S_1-S_0 energy gap and of the oscillator strength requires an extensive post-processing of the computed trajectories involving four-root state-average MS-CASPT2 computations as detailed in the Supporting Information. This unavoidable post-processing makes the computation of statistically relevant sets of trajectories unpractical. For this reason, we focus on two trajectories released from the FC region with no initial kinetic energy and representing limiting cases (see below). These trajectories, have been shown to successfully follow the bottom of the excited state potential energy valley for ZW-NAIP [5b]. For Rh it has also been shown that changing the initial condition do not qualitatively alter the character of the following molecular motion [13].

Acknowledgements

This work was in part supported by Mitsubishi Chemical Corporation. M. O. acknowledges funding from the Center for Photochemical Sciences and the School of Arts & Sciences of Bowling Green State University and S.H. from CNRS and Université de Strasbourg.

[1] a)V. Balzani, A. Credi, M. Venturi, in *Chemical Society Reviews, Vol. 38*, **2009**, pp. 1542; b)T. Hugel, N. B. Holland, A. Cattani, L. Moroder, M. Seitz, H. E. Gaub, *Science* **2002**, *296*, 1103; c)M. Klok, N. Boyle, M. T. Pryce, A. Meetsma, W. R. Browne, B. L. Feringa, *Journal of the American Chemical Society* **2008**, *130*, 10484.

[2] R. W. Schoenlein, L. A. Peteanu, R. A. Mathies, C. V. Shank, *Science* **1991**, *254*, 412.

[3] H. J. A. Dartnall, *Vision Research* **1968**, *8*, 339.

[4] a)I. Ioffe, A. L. Dobryakov, A. A. Granovsky, N. P. Ernsting, J. L. P. Lustres, *Chemphyschem* **2011**, *12*, 1860; b)D. Polli, P. Altoe, O. Weingart, K. M. Spillane, C. Manzoni, D. Brida, G. Tomasello, G. Orlandi, P. Kukura, R. A. Mathies, M. Garavelli, G. Cerullo, *Nature* **2010**, *467*, 440; c)I. Schapiro, M. N. Ryazantsev, L. M. Frutos, N. Ferre, R. Lindh, M. Olivucci, *Journal of the American Chemical Society* **2011**, *133*, 3354; d)R. Siewertsen, J. B. Schoenborn, B. Hartke, F. Renth, F. Temps, *Physical Chemistry Chemical Physics* **2011**, *13*, 1054; e)O. Weingart, P. Altoe, M. Stenta, A. Bottoni, G. Orlandi, M. Garavelli, *Physical Chemistry Chemical Physics* **2011**, *13*, 3645.

[5] a)F. Lumento, V. Zanirato, S. Fusi, E. Busi, L. Latterini, F. Elisei, A. Sinicropi, T. Andruniów, N. Ferré, R. Basosi, M. Olivucci, *Angewandte Chemie International Edition* **2007**, *46*, 414; b)A. Melloni, R. R. Paccani, D. Donati, V. Zanirato, A. Sinicropi, M. L. Parisi, E. Martin, M. Ryazantsev, W. J. Ding, L. M. Frutos, R. Basosi, S. Fusi, L. Latterini, N. Ferré, M. Olivucci, *Journal of the American Chemical Society* **2010**, *132*, 9310.

[6] A. Sinicropi, E. Martin, M. Ryazantsev, J. Helbing, J. Briand, D. Sharma, J. Léonard, S. Haacke, A. Cannizzo, M. Chergui, V. Zanirato, S. Fusi, F. Santoro, R. Basosi, N. Ferré, M. Olivucci, *Proceedings of the National Academy of Sciences of the United States of America* **2008**, *105*, 17642.

[7] a)B. G. Levine, T. J. Martinez, *Annual Review of Physical Chemistry* **2007**, *58*, 613; b)M. A. Robb, F. Bernardi, M. Olivucci, *Pure and Applied Chemistry* **1995**, *67*, 783.

[8] M. Ben-Nun, F. Molnar, K. Schulten, T. J. Martínez, *Proceedings of the National Academy of Sciences of the United States of America* **2002**, *99*, 1769.

[9] a)I. Burghardt, J. T. Hynes, E. Gindensperger, L. S. Cederbaum, *Physica Scripta* **2006**, *73*, C42; b)A. Kahan, A. Wand, S. Ruhman, S. Zilberg, Y. Haas, *Journal of Physical Chemistry a* **2011**, *115*, 10854; c)A. Toniolo, S. Olsen, L. Manohar, T. J. Martinez, *Faraday Discussions* **2004**, *127*, 149; d)A. M. Virshup, C. Punwong, T. V. Pogorelov, B. A. Lindquist, C. Ko, T. J. Martínez, *Journal of Physical Chemistry B* **2009**, *113*, 3280.

[10] Q. Wang, R. W. Schoenlein, L. A. Peteanu, R. A. Mathies, C. V. Shank, *Science* **1994**, *266*, 422.

[11] J. Briand, O. Braem, J. Rehault, J. Leonard, A. Cannizzo, M. Chergui, V. Zanirato, M. Olivucci, J. Helbing, S. Haacke, *Physical Chemistry Chemical Physics* **2010**, *12*, 3178.

[12] J. Léonard, J. Briand, S. Fusi, V. Zanirato, M. Olivucci and S. Haacke, submitted..

[13] L. M. Frutos, T. Andruniow, F. Santoro, N. Ferre, M. Olivucci, *Proceedings of the National Academy of Sciences of the United States of America* **2007**, *104*, 7764.

[14] G. Haran, E. A. Morlino, J. Matthes, R. H. Callender, R. M. Hochstrasser, *Journal of Physical Chemistry a* **1999**, *103*, 2202.

[15] R. C. Haddon, L. T. Scott, *Pure and Applied Chemistry* **1986**, *58*, 137.

[16] P. Kukura, D. W. McCamant, S. Yoon, D. B. Wandschneider, R. A. Mathies, *Science* **2005**, *310*, 1006.

[17] a)K. Andersson, F. Aquilante, M. Barysz, E. Bednarz, A. Bernhardsson, M. R. A. Blomberg, Y. Carissan, D. L. Cooper, M. Cossi, A. Devarajan, L. D. Vico, N. Ferré, M. P. Fülscher, A. Gaenko, L. Gagliardi, G. Ghigo, C. de Graaf, B. A. Hess, D. Hagberg, A. Holt, G. Karlström, J. W. Krogh, R. Lindh, P.-Å. Malmqvist, T. Nakajima, P. Neogrády, J. Olsen, T. B. Pedersen, J. Raab, M. Reiher, B. O. Roos, U. Ryde, B. Schimmelpfennig, M. Schütz, L. Seijo, L. Serrano-Andrés, P. E. M. Siegbahn, J. Stålring, T. Thorsteinsson, V. Veryazov, P.-O. Widmark, A. Wolf, *Vol. version 7.4.*, **2009**; b)G. Karlström, R. Lindh, P.-Å. Malmqvist, B. O. Roos, U. Ryde, V. Veryazov, P.-O. Widmark, M. Cossi, B. Schimmelpfennig, P. Neogrady, L. Seijo, *Computational Materials Science,* **2003**, *28*, 222.

[18] J. W. Ponder, F. M. Richards, *Journal of Computational Chemistry* **1987**, *8*, 1016.

[19] D. A. Case, D. A. Pearlman, J. W. Caldwell, T. E. C. III, J. Wang, W. S. Ross, C. L. Simmerling, T. A. Darden, K. M. Merz, R. V. Stanton, A. L. Cheng, J. J. Vincent, M. Crowley, V. Tsui, H. Gohlke, R. J. Radmer, Y. Duan, J. Pitera, I. Massova, G. L. Seibel, U. C. Singh, P. K. Weiner, P. A. Kollman*, Vol. 7*, **2002**.

[20] F. Melaccio, M. Olivucci, R. Lindh, N. Ferre, *International Journal of Quantum Chemistry* **2011**, *111*, 3339.

[21] W. C. Swope, H. C. Andersen, P. H. Berens, K. R. Wilson, *Journal of Chemical Physics* **1982**, *76*, 637.

[22] L. V. Schäfer, G. Groenhof, M. Boggio-Pasqua, M. A. Robb, H. Grubmüller, *PLoS Computational Biology* **2008**, *4*, e1000034.

Received: ((will be filled in by the editorial staff))
Revised: ((will be filled in by the editorial staff))
Published online: ((will be filled in by the editorial staff))

Entry for the Table of Contents (Please choose one layout only)

Layout 1:

Catch Phrase : Coherent Photomechanical Transduction

Author(s), Corresponding Author(s)* …….…… Page – Page

Title Text

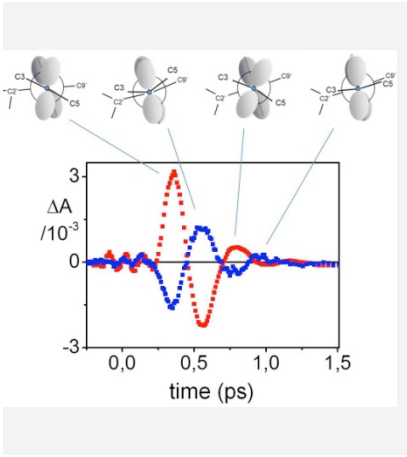

Vibrational coherence and low-frequency oscillations reveal a remarkable property of the IP molecular switches: they convert light into mechanical energy delivered in a few, specific reactive modes. Pronounced out-of-plane motions triggered in the excited state modulate the π-orbital overlap across the twisted C=C bond after the decay to the ground state, leading to the observed oscillations of the S_0-S_1 transition energy.